Frequency Response of Slow and Fast Light in Integrated Semiconductor Waveguide Amplifiers and Absorbers

Filip Öhman and Jesper Mørk
COM•DTU Department of Communications, Optics & Materials, NanoDTU, Technical University of Denmark, Building 343, DK-2800 Kgs. Lyngby, Denmark, fo@com.dtu.dk.

Abstract: *We have investigated slow and fast light in a semiconductor waveguide device with concatenated gain and absorber sections for applications within microwave photonics. A phase shift of 110 degrees and a true-time delay of 150 ps at GHz-frequencies are demonstrated experimentally and investigated theoretically.*

Introduction

The possibility of controlling the propagation speed of light has received a lot of attention lately [1-11]. The effect has been demonstrated using electromagnetically induced transparency (EIT) in ultracold atomic gases [1] as well as coherent population oscillation (CPO) in a ruby crystal [2] and semiconductor structures [3]-[7]. It has been shown that the slow-down of light in saturable absorbers as used in [3]-[7] can also be described by time-dependent absorption saturation [5], [6]. Slow light effects have been demonstrated both using pulses [1], [6] and sine-modulated signals [2], [4], [5], [7], and are envisioned to have applications within several different areas. One of the more spectacular applications is the possibility to store optical pulses in an all-optical buffer. Theoretical predictions [5], [8], however, point toward a finite delay-bandwidth product for these effects, which limits the number of bits that can be stored to just a few. A less demanding, but very relevant, application is the control of optical microwave signals, where a phase delay of the signal is needed in for example optically fed phased array antennas and optical microwave signal processing [9].

Earlier experiments [5] have demonstrated an electrically and optically controllable delay in a single waveguide electro absorber (EA) at high modulation frequency. The EA acts as a saturable absorber and slow light is achieved by CPO, which in this case can also be described by a time varying absorption induced by the intensity modulated signal [5]. The maximum achievable delay is thus limited by the carrier lifetime, and the large residual absorption in the device further limits the achievable delay and introduces substantial losses to the signal. While the existence of a fundamental limitation in terms of a finite delay-bandwidth product is common for both CPO [5, 8] and EIT [8], the loss-limitation of the CPO effect is a main issue that may limit applications. In order to solve these problems we have recently shown that it is possible to utilize a waveguide device with several alternating sections of semiconductor optical amplifiers (SOA) and electro-absorbers (EA) for enhancing the delay and simultaneously achieving optical gain [7]. This also provides the possibility of independent control of the timing and amplitude of the signal. Furthermore, by concatenating several SOA-EA pairs an increase of the absolute value of the controllable time or phase delay is achieved. While the counteraction of the loss using an amplifier seems a trivial solution, the effect on the delay is not. It has been shown that an SOA introduces an advancement of the phase, corresponding to the effect of fast light [5, 10], thus counteracting the effect of the EA. The achievement of a net, sizable, phase change thus relies on a careful choice of the operating conditions of the SOA and the EA. We show below that this is indeed possible and besides resulting in net gain it also allows control of the amplitude of the output signal. In addition, the waveguide device is very compact and is easily integrated into arrays including a light source, modulator and detectors for a complete optical system. We believe this device structure represents a viable route for the use of slow-light effects for a number of practical applications, such as phased-array antennas and microwave filters, while benefiting from standard semiconductor fabrication technology.

In this paper we compare experimental results with an analytical model and investigate the interplay between the amplifying and absorbing sections, including the frequency dependence and true time delay.

The device and experimental setup

The fabricated device, shown in Fig. 1, employs an optical ridge waveguide structure that is angled 7 degrees relative to the cleaved facets, which are also anti reflection coated to further reduce reflections into the waveguide. The electrode on top of the waveguide is divided into sections. The length of the SOA and EA sections are 545 and 120 μm, respectively. Re-growth has been used to realize different active material in the amplifier and absorber sections, respectively. The amplifiers consist of five 7 nm thick, compressively strained, InGaAsP quantum wells, in a strain compensated structure and the absorbers have fifteen 10 nm thick wells. Experiments are made on two different devices, one as shown in Fig. 1 with two SOA-EA pairs and one device with a single pair.

The experiments are performed by sending a sinusoidal intensity modulated light signal through the device under test and measuring the phase and ampli tude of the modulated signal relative to a reference beam using a network analyzer. The reference beam

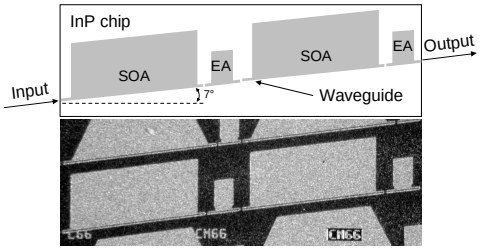

Fig. 1 Photo and schematic of the investigated device. The SOAs and EAs are 545 and 120 µm long, respectively.

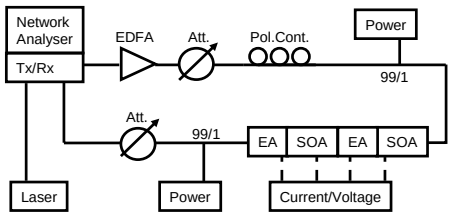

Fig. 2 The experimental setup used in the experiments.

has traversed the same path with the device operated at the desired reference point. For example, the background refractive index can be achived by biasing the device at transparency. The setup is shown in Fig. 2 and more details are given in [5] and [7]. The signal power at the input is controlled by an erbium doped fiber amplifier and a variable attenuator. The devices are not optimized for polarization independent operation and thus a polarization controller is used. The power at the input and output of the device is measured using 1% splitters and power meters.

The model

The model used in this paper for simulating the device is derived by using a wave mixing description [5]. A double-sideband modulated signal, as used in the experiments for validating the model, can be considered as a strong pump signal at the optical carrier angular frequency (ω_0) and a weak probe signal at the modulation sideband $\omega_1 = \omega_0 \pm \Omega$, where Ω is the modulation angular frequency. In order to compare the calculations to experiments the phase change of the modulated signal is calculated using

$$\Delta\varphi_{\mathrm{mod}} = \Omega \Delta t_{\mathrm{mod}} = \Omega \frac{L}{c}\left(\bar{n}_{\mathrm{mod}} - n_{gb}\right), \qquad (1)$$

where L is the length of the section, c is the speed of light in vacuum and n_{gb} is the background group index. The modulation index taking both sidebands into consideration and averaged over the length of the section is [5]

$$\bar{n}_{\mathrm{mod}} = n_{gb} - \frac{c}{L}\frac{1}{\Omega}\mathrm{Arctan}\left\{\frac{\Omega\tau_s (T_{sat}-1)P(0)/P_{sat}}{(\Omega\tau_s)^2 + 1 + (T_{sat}+1)P(0)/P_{sat} + T_{sat}(P(0)/P_{sat})^2}\right\}, \qquad (2)$$

where τ_s is the effective carrier lifetime, P_{sat} is the saturation power and $P(0)$ is the power at the input of the section. The saturated intensity transmission is given by the implicit expression

$$\ln(T_{sat}) + (T_{sat}-1)\frac{P(0)}{P_{sat}} = \Gamma g_0 L, \qquad (3)$$

where g_0 is the unsaturated gain and Γ is the confinement factor.

The parameters for the absorber sections depend on the reverse bias voltage. These effects are accounted for in a phenomenological way by introducing the following dependencies on reverse bias voltage, V:

$$g_0 = -a_V\left(V - V_{on}\right)^2, \qquad (4)$$

$$\tau_s = \tau_{s0}\exp(-V/V_{ref}), \qquad (5)$$

$$P_{sat} = P_{sat,0}\exp(V/V_{ref}), \qquad (6)$$

where a_V, V_{on}, τ_{s0}, $P_{sat,0}$ and V_{ref} are constants. These approximations are only valid for a limited range of reverse bias voltages. The amplifier sections are described by constant g_0, P_{sat} and τ_s, corresponding to a constant bias current.

More details of the model for a single EA section are presented in [5] and for this work we have extended the model to include multiple sections with absorption or gain. The gain sections model is derived using the same general assumptions as for the absorbers and the main difference is the choice of parameter values.

Results

In Fig. 3 the measured frequency response of the phase shift in two SOA-EA pairs is displayed. The reference phase is measured at an EA bias of 0 V, input power of 5.3 dBm and SOA bias current of 120 mA to each section. During the measurement the power and SOA bias is kept constant while the bias voltage to the two absorber sections is varied. An adjustable phase shift relative to the reference of up to 110 degrees is measured around 4 GHz. At higher frequencies the limited response time of the device due to a finite carrier lifetime results in smaller phase shifts. At large reverse bias the net absorption is high and detector noise becomes detrimental to the signal.

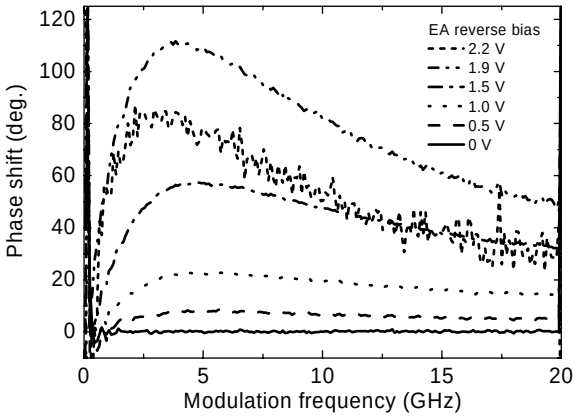

Fig. 3 Measured phase shift for different bias voltages to the two EAs, relative to an EA bias of 0 V. The input power was 5.3 dBm and the bias current 120 mA to each SOA section.

For applications in microwave photonics and in particular phased arrayed antennas it is important to have a phase shift which depends on modulation frequency as $\Delta\phi(\Omega) = \Delta\phi_0\Omega/\Omega_c$ [9], where Ω_c

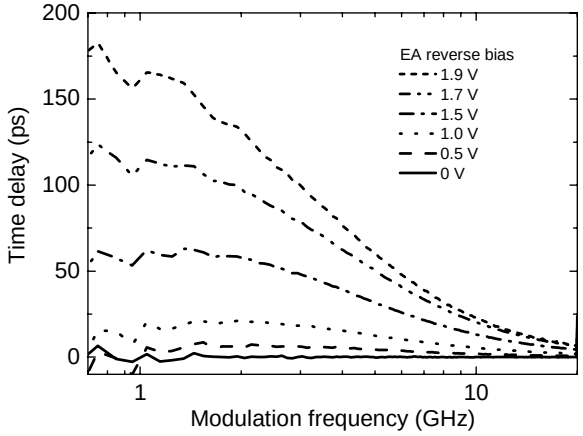

Fig. 4 Measured time delays as function of modulation frequency for different bias voltages to the two EAs.

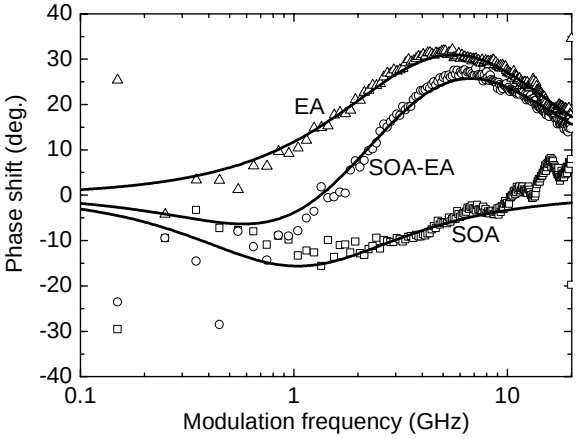

Fig. 5 Measured and calculated phase shift relative the background group index for a SOA-EA pair compared to a single SOA and a single EA. The SOA bias is 120 mA, the EA reverse bias is 0.7 V and the input power is 5.3 dBm.

is the microwave carrier frequency and $\Delta\phi_0$ is the phase shift achieved at this frequency. This translates into a so-called true-time delay which is constant, $\Delta t=\Delta\phi/\Omega$, for the whole signal bandwidth. The true-time delay corresponding to the measured phase shift is plotted in Fig. 4. A maximum time delay of 165 ps is measured at low modulation frequency. The time delay falls off rather quickly with modulation frequency resulting in a bandwidth of a few GHz.

The interplay between the delays in the SOA and the EA in dependence of the modulation frequency is investigated in Fig. 5. The phase shift in one SOA-EA pair as function of modulation frequency is compared to that of an EA section and that of an SOA section. For the measurements on the SOA-EA pair the phase shift is measured with reference to the background group index achieved by biasing the whole device at transparency. When measuring the single SOA the bias to the EA is kept at transparency and the bias to the SOA was 120 mA. When measuring the single EA the reference measurement was made with the SOA biased at 120 mA and the EA at transparency. The input power to the SOA was in all cases 5.3 dBm.

The results in Fig. 5 demonstrate that the gain and absorber sections have opposite responses for the induced microwave phase shift. In the absorber the signal is delayed due to a slowing down of the group velocity, while in the amplifier the group velocity is increased. The two opposite responses can however be separated by utilizing the fact that the fast sweep-out time of the carriers in the EA results in a phase shift that reaches maximum at higher frequencies in the EA than in the SOA, which has a longer carrier lifetime. This combined with an input saturation power in the EA that is lower than the output saturation power of the SOA results in a dominating slow light response from the EA in the component, especially at high frequencies, as seen in Fig. 5.

In the experiments in Fig. 3 the reference is chosen at a high input power, large SOA bias current and zero bias voltage to the EAs. The result is a push-pull effect where the reference is chosen at an operation point where the fast light effect in the SOAs is large and the slow light effect in the EAs is low. As the bias to the EAs is increased the slow light effect is enhanced while the higher absorption leads to lower input power to the second SOA and hence a smaller fast light effect. In total this gives a relative phase shift in the same direction in both EAs and the second SOA, leading to a larger delay relative to the reference. This operation mode also removes the fast light effect at low modulation frequencies, seen in Fig. 5 and results in a constant true-time delay as seen in Fig. 4.

In the model the EA and SOA parameters are chosen to give a good fit of the measured phase shift (Fig. 5) and gain (Fig. 6) of the SOA and EA. The input power to the SOA is 5.3 dBm and coupling losses are estimated to 3 dB. The background group index is n_{gb}=3.4 and for the SOAs Γ=0.065, g_0= 700 cm^{-1}, τ_s= 250 ps and P_{sat}= 7 mW. The EA parameter values are Γ=0.2, a_V= 8.5×10^4 V^{-2}m^{-1}, V_{on}= -0.9 V, V_{ref}= 2 V, τ_{s0}= 110 ps and $P_{sat,0}$= 1.5 mW. The model shows good agreement with the experiments in Fig. 5. However, when calculating the phase shift for the same conditions as in Fig. 3 only a qualitative agreement is achieved, as seen in Fig. 7. The model does not quite reproduce the maximum phase shift obtained experimentally and the maximum phase shift is achieved at a lower bias voltage. Furthermore the model displays a somewhat larger change in the position of the maximum phase shift towards lower modulation frequencies as the bias voltage is increased.

In the model, saturation effects due to the amplified spontaneous emission from the SOAs is not included and neither is the finite reflections at the facets. The model for the EAM is, as mentioned before, based on phenomenological assumptions that do not hold well for large reverse bias, which can be seen in Fig. 6 where the gain of the fitted model is compared to the experiments. At reverse biases of more than about 1 V the quadratic dependence of the absorption on the

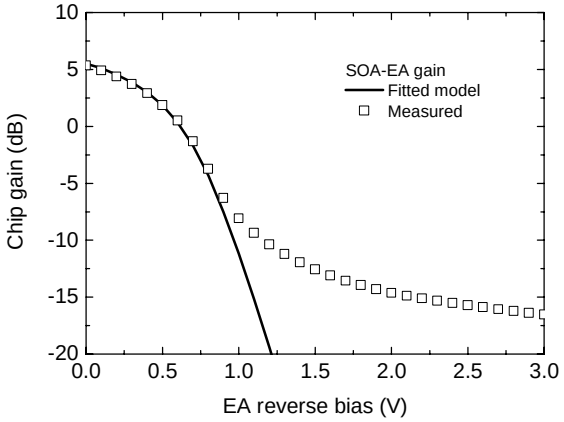

Fig. 6 Measured and calculated chip gain of the SOA-EA device. The SOA bias is 120 mA and the EA reverse bias is 0.7 V.

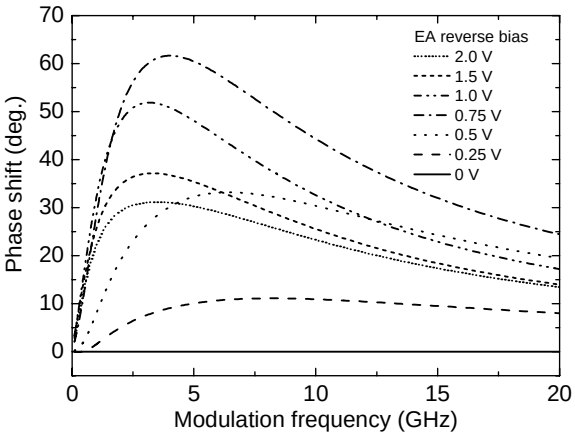

Fig. 7 Calculated phase shift (relative to an EA bias of 0 V) for different values of the bias voltage to the two EAs. The input power was 5.3 dBm.

bias in the EA model results in far too large absorption. This could to some degree account for the discrepancies between the model and experiments. In addition to the absorption, the voltage dependence of the sweep-out time and saturation power could also benefit from a more detailed model and potentially give a better quantitative agreement.

Conclusions

We have performed experiments and developed a theoretical model to investigate the frequency dependence of slow light in a semiconductor wave guide with alternating gain and absorber sections. The model agrees qualitatively with the experimental results but a more detailed model is required for better quantitative agreement. The investigations demonstrate the feasibility of achieving large true-time delay by cascading several sections and operating in a push-pull mode. The use of alternating gain and absorber sections also give the potential for simultaneous control of the modulation amplitude as well as tailoring of the frequency response. The device thus demonstrates good potential for applications within microwave photonics.

Acknowledgments

This work was supported by the Danish Research Council for Technology and Production Sciences.

References

1 L. V. Hau, S. E. Harris, Z. Dutton and C. H. Behroozi, “Light speed reduction to 17 meters per second in an ultracold atomic gas.” Nature 397, 594—598 (1999).

2 M. S. Bigelow, N. N. Lepeshkin and R. W. Boyd, “Observation of ultraslow light propagation in a ruby crystal at room temperature.” Phys. Rev. Lett. 90, 113903-1-4 (2003).

3 J. C. Chang-Hasnain, P.-C. Ku, J. Kim and S.-L. Chuang, “Variable optical buffer using slow-light in semiconductor nanostructures.” Proc. IEEE 91, 1884 (2003).

4 P. Palinginis, S. Crankshaw and F. Sedgwick, “Ultra-slow light (<200 m/s) propagation in a semiconductor nanostructure. Appl. Phys. Lett. 87, 171102 (2005).

5 J. Mørk, R. Kjær, M. van der Poel and K. Yvind, “Slow light in a semiconductor waveguide at gigahertz frequencies.” Opt. Express 13, 8136-8145 (2005).

6 M. v.d. Poel, J. Mørk and J. M. Hvam, “Controllable delay of ultrashort optical pulses in a semiconductor quantum dot amplifier.” Opt. Express 13, 8032-8037 (2005).

7 Filip Öhman, Kresten Yvind, and Jesper Mørk, “Voltage-controlled slow light in an integrated semiconductor structure with net gain”, Opt. Express, Vol. 14, Issue 21, pp. 9955-9962, (2006).

8 R. S. Tucker, P.-C. Ku and C. J. Chang-Hasnain, “Slow-light optical buffers: capabilities and fundamental limitations.” J. Lightwave Technol. B, 4046 (2005).

9 I. Frigyes and A. J. Seeds, “Optically Generated True-Time Delay in Phased-Array Antennas” Trans. Microwave Theory and Techniques, Vol. 43 pp. 2378-2386 (1995).

10 M. S. Bigelow, N. N.Lepeshkin and R. W. Boyd, “Superluminal and Slow Light Propagation in a Room-Temperature Solid.” Science 301, 200-202 (2003).

11 H. Su and S. L. “Chuang Room temperature slow and fast light in quantum-dot semiconductor optical amplifiers” App. Phys. Lett., Vol 88, 061102 (2006)